Organic-Acid-Catalyzed Sol–Gel Route for Preparing Poly(methyl Methacrylate)–Silica Hybrid Materials

Jui-Ming Yeh, Kuan-Yeh Huang, Chung-Feng Dai, B. G. Chand, Chang-Jian Weng

Department of Chemistry and Center for Nanotechnology at CYCU, Chung Yuan Christian University, Chung Li 32023, Taiwan, Republic of China

Received 7 January 2008; accepted 20 May 2008
DOI 10.1002/app.28778
Published online 7 August 2008 in Wiley InterScience (www.interscience.wiley.com).

ABSTRACT: In this study, a series of organic–inorganic hybrid sol–gel materials consisting of a poly(methyl methacrylate) (PMMA) matrix and dispersed silica (SiO_2) particles were successfully prepared through an organic-acid-catalyzed sol–gel route with *N*-methyl-2-pyrrolidone as the mixing solvent. The as-synthesized PMMA–SiO_2 nanocomposites were subsequently characterized with Fourier transform infrared spectroscopy and transmission electron microscopy. The solid phase of organic camphor sulfonic acid was employed to catalyze the hydrolysis and condensation (i.e., sol–gel reactions) of tetraethyl orthosilicate in the PMMA matrix. The formation of the hybrid membranes was beneficial for the physical properties at low SiO_2 loadings, especially for enhanced mechanical strength and gas barrier properties, in comparison with the neat PMMA. The effects of material composition on the thermal stability, thermal conductivity, mechanical strength, molecular permeability, optical clarity, and surface morphology of the as-prepared hybrid PMMA–SiO_2 nanocomposites in the form of membranes were investigated with thermogravimetric analysis, differential scanning calorimetry, dynamic mechanical analysis, gas permeability analysis, ultraviolet–visible transmission spectroscopy, and atomic force microscopy, respectively. © 2008 Wiley Periodicals, Inc. J Appl Polym Sci 110: 2108–2114, 2008

Key words: atomic force microscopy (AFM); FT-IR; nanocomposites; TEM

INTRODUCTION

Recently, organic–inorganic hybrid sol–gel materials have become a unique class of high-performance materials in industrial and academic research because of the integration of the properties of both organic polymers (i.e., flexibility, low density, toughness, and formability) and ceramics (i.e., excellent mechanical and optical properties such as surface hardness, modulus, strength, and transparency and a high refractive index). There are numerous reports in the literature associated with the preparation of organic–inorganic hybrid materials using sol–gel technology.[1–8]

In sol–gel technology, organosilicates, organotitanates, organoaluminates, and so forth are typically hydrolyzed into multihydroxyl compounds, which subsequently condense into gel-like structures that can be further dried and fired into ceramic coatings, foams, or monolithic objects. The representative example for the sol–gel process is the hydrolysis of tetraethyl orthosilicate (TEOS) to produce silica (SiO_2) and ethanol as a volatile and easily removed byproduct. Acids, bases, and even some salts are usually required to catalyze the sol–gel process effectively. Currently, a considerable number of literature reports are associated with the preparation of organic–inorganic hybrid materials using aqueous inorganic acids (e.g., aqueous HCl) or bases (e.g., aqueous NaOH and aqueous NH_4OH) as catalysts by the sol–gel pathway. Recently, Yeh et al.[9] reported the preparation of polymer–SiO_2 hybrid materials through an organic-base-catalyzed sol–gel route. In that case, aniline monomers were adopted not only as organic base catalysts to catalyze the sol–gel reactions of TEOS but also as dispersing agents during the preparation of the hybrid materials. On the other hand, the preparation of organic–inorganic hybrid sol–gel materials can also be carried out by photochemical synthesis with photoacids, such as diphenyliodonium chloride and triphenylsulfonium hexafluoroantimonate, as catalysts under UV radiation.[10,11] However, organic–inorganic hybrid materials prepared through the organic-acid-catalyzed sol–gel route have seldom been mentioned.

In this work, we present the preparation of poly (methyl methacrylate) (PMMA)–SiO_2 hybrid materials through the effective dispersion of inorganic SiO_2 particles into a commercial PMMA matrix through a solid organic acid [e.g., D-(+)-10-camphorsulfonic acid (CSA)] catalyzed sol–gel route. The as-synthesized hybrid sol–gel materials were subsequently characterized with Fourier transform infrared (FTIR)

Correspondence to: J.-M. Yeh (juiming@cycu.edu.tw).
Contract grant sponsor: National Science Council of the Republic of China, Taiwan, and the Ministry of Education, Taiwan, Republic of China; contract grant number: NSC 94-2113-M-033-008.

spectroscopy and transmission electron microscopy (TEM). The effects of the material composition on the thermal stability, thermal conductivity (T_c), mechanical strength, molecular permeability, optical clarity, and surface morphology of the as-prepared hybrid PMMA–SiO_2 sol–gel materials in the form of membranes were investigated with thermogravimetric analysis (TGA), differential scanning calorimetry (DSC), dynamic mechanical analysis (DMA), gas permeability analysis (GPA), ultraviolet–visible (UV–vis) transmission spectroscopy, and atomic force microscopy (AFM), respectively.

EXPERIMENTAL

Materials and instruments

PMMA (weight-average molecular weight = 350,000; Aldrich, USA), TEOS (Fluka, Germany), CSA (Acros, USA), and *N*-methyl-2-pyrrolidone (NMP; HPLC grade; Mallinckrodt, USA) were used as received without further purification.

FTIR spectra were measured on pressed KBr pellets with a Jasco FT/IR-460 Plus spectrometer. The sample for TEM study was first prepared by the placement of the film of the hybrid sol–gel materials into epoxy resin capsules followed by the curing of the epoxy resin at 100°C for 24 h in a vacuum oven. Then, the cured epoxy resin containing hybrid sol–gel materials was microtomed with a Reichert-Jung Ultracut-E (Heidelberg, Germany) into 60–90-nm-thick slices. Subsequently, one layer of carbon about 10 nm thick was deposited onto these slices on 100-mesh copper nets for TEM observations on a JEOL 200FX (Japan) with an acceleration voltage of 120 kV. A Du Pont thermal analysis system equipped with a TGA Q-50 (USA) thermogravimetric analyzer and a DSC Q-10 (USA) differential scanning calorimeter were employed for the thermal analyses under air flow. The programmed heating rate was 10°C/min. The DMA Q-800 (USA) dynamic mechanical analyzer was employed for the mechanical analyses at a heating rate of 3°C/min. T_c was measured in the thin film mode with a transient plane source (TPS) (hot disk, TechMaz, Switzerland). A Yanagimoto Co., Ltd. (Japan), gas permeability analyzer (model GTR 10) was employed to perform the permeation experiments with oxygen gas and water vapor. UV–vis transmission spectra were obtained with a Hitachi U-2000 UV–vis spectrometer (Hitachi U-2000, Japan), AFM (model DI 5000, Digital Instrument, Inc., USA) was used to probe the surface morphology of the neat polymer and hybrid sol–gel films.

Preparation of the PMMA–SiO_2 hybrid membranes

Representative steps for preparing PMMA–SiO_2 hybrid sol–gel materials (PMS01) were as follows. Solid CSA (0.6 mg) was first dissolved in approximately 14 g of NMP by an ultrasonic bath for at least 1 h to promote the solubility of CSA in NMP (denoted by beaker A). TEOS (60 mg) was then gradually added to beaker A. The mixture was stirred at room temperature for another 24 h. Subsequently, 1.94 g of commercial PMMA powder (weight-average molecular weight = 350,000) was introduced into the previous as-prepared mixing solution. The resultant mixed PMMA–SiO_2 hybrid solution was further stirred until a homogeneous, clear solution was obtained. The as-prepared solution was subsequently filtered with a 0.45-μm hydrophilic poly(vinylidene fluoride) filter (Millev-Hv, Millipore, India) and cast onto a 5 cc/pcs glass plate (5 cm × 5 cm). The as-prepared hybrid sample was then treated with conditioning at 80°C for 1 h, 120°C for 7 h and 150°C for 1 h in an oven to allow the evaporation of NMP. A series of PMMA–SiO_2 hybrid sol–gel membranes were then obtained by detachment from the inorganic glass plate.

Gas barrier properties of the membranes

The gas permeability of the neat PMMA and a series of hybrid membranes was determined with a Yanco GTR-10 gas permeability analyzer. The gas permeability was calculated according to the following equation:

$$P = l/(p_1 - p_2) \times [(q/t)/A]$$

where P is the gas permeability [cm^3 (STP) cm cm^{-2} s^{-1} $cmHg^{-1}$]; q/t is the volumetric flow rate of the gas permeate [cm^3 (STP)/s]; l is the membranes thickness (cm); A is the effective film area (cm^2); and p_1 and p_2 are the high and low pressures (cmHg), respectively, in the sides of the membrane. The rate of transmission of O_2 was obtained by gas chromatography, from which the O_2 permeability was calculated. On

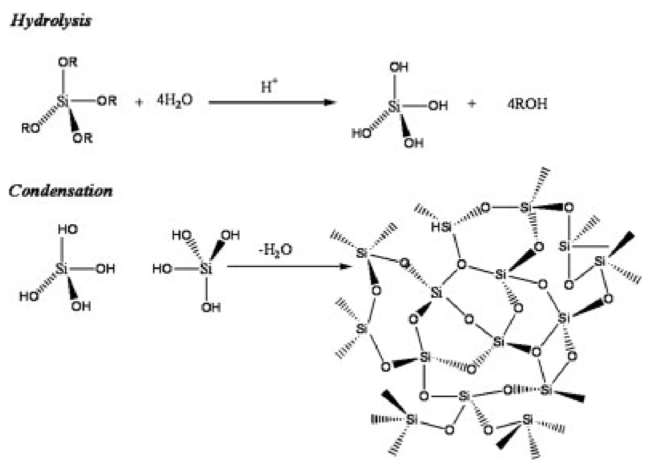

Scheme 1 General equations for the sol–gel reactions of TEOS.

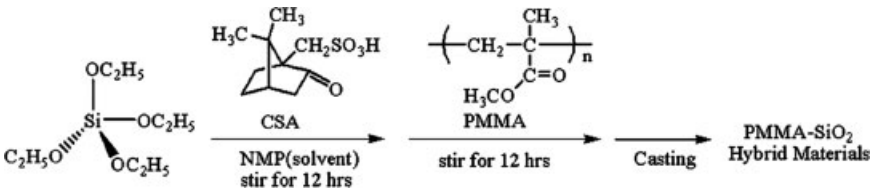

Scheme 2 Flowchart for the preparation of the PMMA–SiO_2 nanocomposite materials.

the other hand, the H_2O permeability experiment was performed with an apparatus similar to that mentioned in our previously published article,[12] in which the feed solution was not in contact with the membrane. The feed solution was vaporized first and subsequently permeated through the membrane with an effective area of approximately 10.2 cm^2. The permeation rate was determined by the measurement of the permeate weight.

RESULTS AND DISCUSSION

The traditional sol–gel process involves the hydrolysis and condensation of TEOS to form amorphous silicate (SiO_2) networks. Similar reactions can also be carried out with the corresponding orthotitanates and orthozirconates to form TiO_2 and ZrO_2, respectively. The general equations for the sol–gel reactions of a representative example, TEOS, are illustrated in Scheme 1.

In this study, a solid organic acid (CSA) was employed as a catalyst instead of a commonly used liquid inorganic acid (e.g., aqueous HCl) to catalyze the sol–gel reactions. A series of PMMA–SiO_2 hybrid sol–gel materials were then prepared, and the sequential steps are given in Scheme 2.

Characterization

Representative FTIR absorption spectra of the neat PMMA and a hybrid material (e.g., PMS03) are shown in Figure 1. The characteristic absorption peaks of PMMA appearing near 1422 and 1389 cm^{-1} correspond to anti-asymmetric bending for the OCH_3 group and asymmetric bending for the α-CH_3 group, respectively.[13] A sharp peak appearing at 1733 cm^{-1} is associated with the stretching of the C=O group.[14] The bands around 1080 cm^{-1}, corresponding to Si—O—Si linkages, can also be observed in all hybrid sol–gel materials.[15] An absorption band of medium intensity appearing at 1247 cm^{-1} can probably be assigned to the stretching of CH_2—Si.

The morphology of the PMMA–SiO_2 hybrid material was investigated with TEM. TEM images of the CSA-catalyzed PMMA–SiO_2 hybrid sol–gel materials are shown in Figure 2. To exclude the possibility of a catalyzing effect on the sol–gel reactions from the basicity of the organic solvent (i.e., NMP), a free-standing film made from the mixing solution containing PMMA and 3 wt % TEOS dissolved in NMP without the addition of CSA was also prepared as a control experiment. However, we did not find any

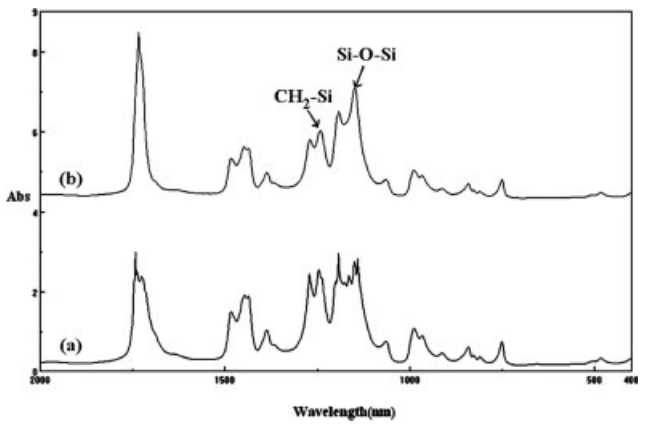

Figure 1 Representative FTIR absorption spectra of (a) PMMA and (b) PMS03.

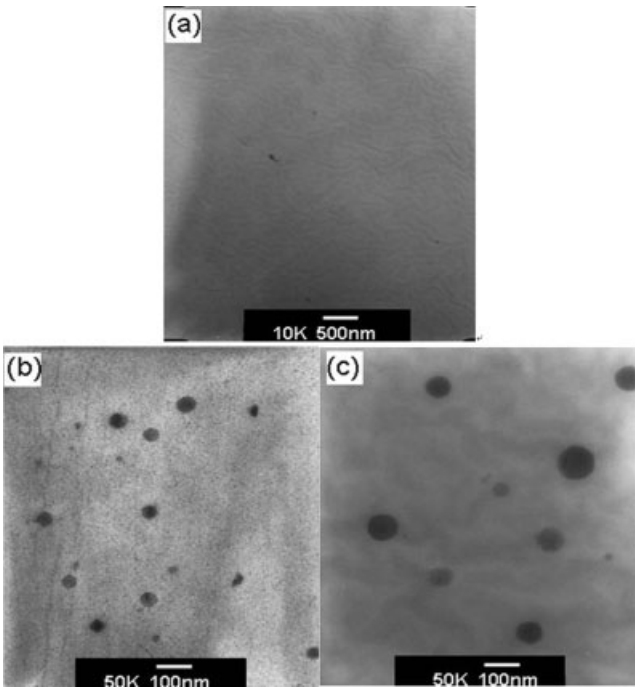

Figure 2 TEM images of the nanocomposite materials for (a) PMMA–TEOS 3% without CSA (10,000×), (b) PMS01 (50,000×), and (c) PMS03 (50,000×).

TABLE I
Thermal Stability, T_c, Mechanical Strength, and Optical Clarity of the Organic-Acid-Catalyzed PMMA–SiO_2 Hybrid Sol–Gel Membranes

	Feed composition (wt %)						
Sample code	PMMA	TEOS	T_d (°C)[a]	T_g (°C)[b]	T_c (W/mk)[c]	Storage modulus (MPa)[d]	Transparency (%)[e]
PMMA	100	0	352.07	95.18	0.2285	2313	92.43
PMS01	99	1	359.09	98.50	0.2128	3410	91.32
PMS02	98	2	361.19	102.89	0.2085	3420	90.92
PMS03	97	3	362.57	102.89	0.2019	3403	90.83

[a] As measured by TGA. T_d was the temperature value at 5% weight loss.
[b] As measured by DSC.
[c] As measured by TPS, transient plane source (hot disk) at 25°C.
[d] As measured by DMA at 30°C.
[e] As measured by UV–vis transmission spectra at 800 nm.

SiO_2 particles in the polymer network through observations of the TEM micrograph, and this indicated that no sol–gel reactions of TEOS catalyzed by NMP occurred in the PMMA matrix without the addition of CSA as a catalyst, as shown in Figure 2(a). However, with the addition of CSA as an acidic catalyst, a well-dispersed phase of SiO_2 particles approximately 60 nm in diameter was obviously formed in the PMMA matrix (e.g., PMS01), as shown in Figure 2(b). Moreover, TEM was also used to further study the microstructures of the hybrid sol–gel materials at higher TEOS loadings. We found that the size of the SiO_2 particles that formed in the polymer matrix increased with the TEOS loading increasing, as shown in Figure 2(c). For example, PMS03 [Fig. 2(c)] revealed an average particle size of dispersed SiO_2 around 100 nm.

Thermal stability and T_c of the membranes

TGA thermograms of the weight loss as a function of temperature for PMMA and a series of hybrid sol–gel materials were studied under an air atmosphere. The TGA results are summarized in Table I. Evidently, the thermal decomposition temperature (T_d) of the hybrid sol–gel materials (e.g., T_d of PMS01 $\sim$ 359°C) shifted toward a higher temperature range than that of PMMA ($T_d \sim$ 352°C), and this confirmed the enhancement of the thermal stability of PMMA by the incorporation of inorganic SiO_2 particles. Furthermore, DSC results for neat PMMA and a series of hybrid sol–gel materials are also listed in Table I. PMMA exhibited an endotherm at approximately 95°C corresponding to the glass-transition temperature (T_g) of PMMA. All the hybrid sol–gel materials showed an increase in T_g (e.g., T_g of PMS01 $\sim$ 98°C) compared to that of PMMA, and this indicated that the incorporation of SiO_2 particles into the polymer matrix via the CSA-catalyzed sol–gel pathway also enhanced T_g of PMMA. In addition to the investigation of common thermal properties such as T_d and T_g on the basis of TGA and DSC measurements, T_c measurement of the as-prepared materials is also an important and interesting research topic. The T_c values of PMMA and a series of hybrid sol–gel materials were measured with a transient plane source (hot disk), as shown in Figure 3, and the data are listed in Table I. The incorporation of SiO_2 particles into the PMMA matrix led to a decrease in T_c of the hybrid sol–gel materials (e.g., T_c of PMS01 = 0.2128 W/mK) versus that of the neat PMMA (T_c = 0.2285 W/mK). The further increase in the SiO_2 concentration in the hybrid films corresponded to a much lower value of T_c. All the T_c data were measured and repeated at least three times to ensure reproducible results. T_c of bulk SiO_2 is 1.4 W/mK,[16] but T_c (i.e., the thermal transport) of nanoscale SiO_2 particles is totally different from that of bulk SiO_2. In this study, we found that T_c of nanoscale SiO_2

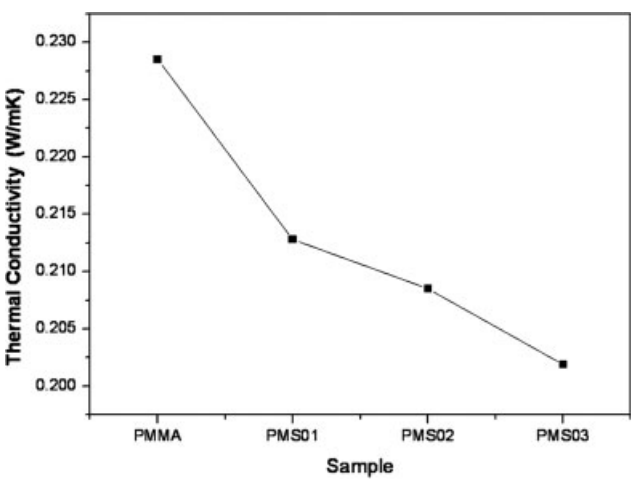

Figure 3 T_c of PMMA and a series of PMS hybrid sol–gel materials as measured by a hot disk.

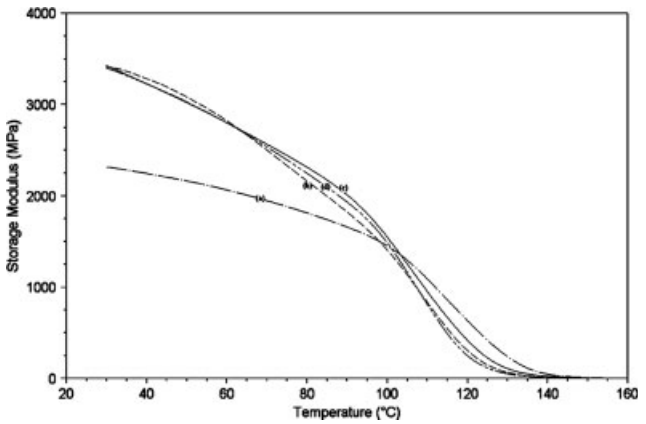

Figure 4 DMA curves of PMMA and a series of hybrid sol–gel membranes: (a) PMMA, (b) PMS01, (c) PMS02, and (d) PMS03.

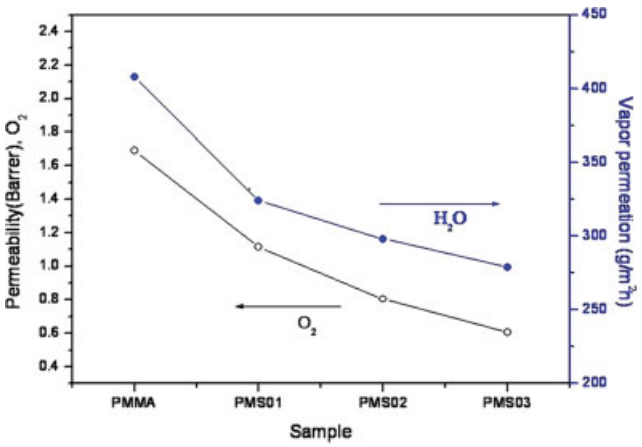

Figure 5 Permeability of O_2 and water vapor as a function of SiO_2 content in the hybrid membranes. [Color figure can be viewed in the online issue, which is available at www.interscience.wiley.com.]

should be significantly lower than that of neat PMMA. The lowering of T_c in nanoscale SiO_2 particles may be explained with reference to the nanowires of semiconductor materials and interpreted as follows. Because of the large surface area to volume ratio and small diameter, phonon (i.e., lattice vibration) boundary scattering in nanoparticles is much stronger than that in bulk materials, and this leads to a reduced phonon mean free path and reduced T_c for nanoparticles.[17]

Mechanical properties of the membranes

The DMA measurements based on storage modulus studies of neat PMMA and a series of hybrid sol–gel films are given in Figure 4, and the data are summarized in Table I. The storage modulus increased with an increase in the SiO_2 loading up to 3 wt %. For example, the storage modulus of the hybrid sol–gel film PMS01 was remarkably increased by 47.4% (from 2313 MPa for neat PMMA to 3410 for PMS01) around 30°C. Moreover, a further increase in the SiO_2 concentration resulted in further enhanced mechanical strength of the hybrid sol–gel materials (e.g., storage modulus of PMS02 = 3420 MPa). The hybrid materials exhibited a significant increase in the storage modulus with the increase in the SiO_2 content during the entire monitoring temperature range, and this may have been due to the fact that a higher SiO_2 loading in the polymer matrix led to a larger interfacial area between the organic and inorganic phases.

Barrier properties of the membranes

Films 190 ± 5 μm thick were made to measure the molecular permeability of the neat PMMA and hybrid sol–gel membranes. For the H_2O vapor permeability studies, we found that the incorporation of SiO_2 into the PMMA matrix resulted in a reduction of the H_2O vapor permeability for the hybrid membranes, as shown in Figure 5 and Table II. A further increase in the SiO_2 concentration resulted in a further enhancement of the molecular barrier property

TABLE II
Gas Permeability and Surface Roughness Properties of the Organic-Acid-Catalyzed PMMA–SiO_2 Hybrid Sol–Gel Membranes

Sample code	Gas permeability		Thickness (μm)[c]	R_a (nm)[d]	R_q (nm)[d]
	H_2O (g h · m^2)[a]	O_2 (Barrer)[b]			
PMMA	408	1.688	186	1.169	1.443
PMS01	324	1.116	195	—	—
PMS02	298	0.804	190	—	—
PMS03	279	0.607	181	0.842	1.138

[a] As measured by VPA (vapor permeability analysis).
[b] As measured by GPA.
[c] As measured by a digimatic micrometer.
[d] As measured by AFM. R_a and R_q are the average and root mean square roughness, respectively.

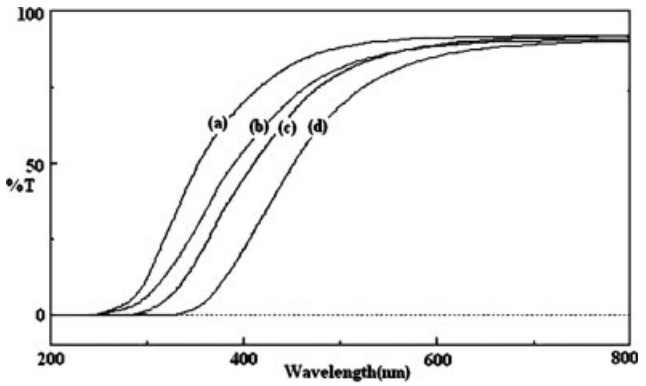

Figure 6 UV–vis transmission spectra of PMMA and a series of hybrid sol–gel membranes: (a) PMMA, (b) PMS01, (c) PMS02, and (d) PMS03.

of the PMS hybrid membranes. For example, the O_2 barrier of the membrane was decreased by 96.5% in permeability (from 1.688 barrer for PMMA to 0.061 barrer for PMS03). The decrease in the gas permeability of the hybrid membrane compared to that of the neat PMMA may be associated with hybrid membranes having a dispersion of SiO_2 spheres in the PMMA matrix. This probably occurred because the barrier properties were governed by the fact that a considerable number of well-dispersed tiny SiO_2 particles ($\sim$ 100 nm) were dispersed in the composite,[18] which led to longer tortuosity of the diffusion pathway of oxygen and water.[19,20]

Optical clarity of the membranes

The optical clarity of free-standing films of PMMA and a series of hybrid sol–gel materials was evaluated and compared through studies with UV–vis transmission spectroscopy. First, we found that the neat PMMA membrane showed high clarity, as shown in Figure 6(a). For example, during the monitoring of the entire visible-light wavelength range (i.e., 400–700 nm), the wavelength at 800 nm for the neat PMMA membrane corresponded to a high optical transmission of approximately 92%. By the incorporation of a SiO_2 particle loading up to 3 wt %, the optical clarity of the hybrid membranes revealed a slight decrease, but it was still very close to the optical transmission of 90%.

Surface morphology of the hybrid membranes

AFM was applied to investigate the surface profiles of the samples. The surface morphology of the hybrid membranes was investigated by AFM in a contact mode, as shown in Figure 7, which exhibits three-dimensional topographical features of the neat polymer PMMA [Fig. 7(a)] and hybrid sol–gel material PMS03 [Fig. 7(b)]. On the basis of the three-dimensional image analysis, a slight, smooth increase in the topography as the polymer PMMA matrix was incorporated with a 3 wt % loading of inorganic SiO_2 was demonstrated The average roughness (R_a) and root mean square roughness (R_q) of the PMMA and PMS03 samples are summarized in Table II, and they suggest that the hybrid sol–gel materials might have no organic–inorganic phase separation. Therefore, the incorporation of a low SiO_2 concentration into the polymer matrix could effectively enhance the flatness.[21]

CONCLUSIONS

In this study, we examined the preparation of PMMA–SiO_2 hybrid materials through an organic-acid (CSA)-catalyzed sol–gel route with NMP as the mixing solvent. All the hybrid materials revealed slightly enhanced thermal stability compared to that of neat PMMA through the evaluation of DSC and TGA studies. Furthermore, the incorporation of SiO_2 nanoparticles into the PMMA matrix led to significant improvements of some physical properties, such as T_c,

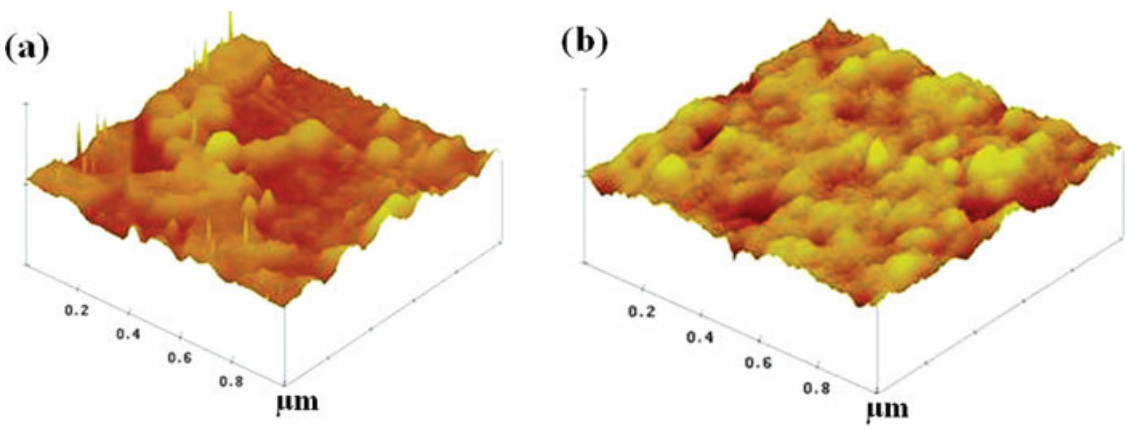

Figure 7 AFM surface images (1 × 1 μm^2) of the (a) PMMA and (b) PMS03 membranes. [Color figure can be viewed in the online issue, which is available at www.interscience.wiley.com.]

the storage modulus, and the gas barrier. Moreover, a low loading of SiO_2 particles in the hybrid sol–gel film showed little effect on the optical transparency of the film. For the surface morphological studies, we found that the incorporation of a low SiO_2 concentration into the polymer matrix (e.g., PMS03) could effectively enhance the flatness of the surface.

The authors thank the Center-of-Excellence Program on Membrane Technology.

References

1. Huang, Z. H.; Qiu, K. Y. Polymer 1997, 38, 521.
2. Wei, Y.; Jin, D.; Yang, C.; Kels, M. C.; Qiu, K. Y. Mater Sci Eng C 1998, 6, 91.
3. Chang, T. C.; Wang, Y. T.; Hong, Y. S.; Chiu, Y. S. Thermochim Acta 2001, 372, 165.
4. Chan, C. K.; Chu, I. M.; Lee, W. Chin, W. K. Macromol Chem Phys 2001, 202, 911.
5. Xie, T.; Zhou, C.; Feng, S.; Wang, X. J Appl Polym Sci 2000, 75, 379.
6. Landry, C. J. T.; Coltrain, B. K.; Brady, B. K. Polymer 1992, 33, 1486.
7. Landry, C. J. T.; Coltrain, B. K.; Wesson, J. A.; Zumbulyadis, N.; Lippert, J. L. Polymer 1992, 33, 1496.
8. Chan, C. K.; Peng, S. L.; Chu, I. M.; Ni, S. C. Polymer 2001, 42, 4189.
9. Yeh, J. M.; Hsieh, C. F.; Yeh, C. W.; Wu, M. J.; Yang, H. C. Polym Int 2007, 56, 343.
10. Wei, Y.; Wang, W.; Yeh, J. M.; Wang, B.; Yang, D.; Murray, J. K., Jr. Adv Mater 1994, 6, 372.
11. Xu, C.; Eldada, L.; Wu, C.; Norwood, R. A.; Shacklette, L. W.; Yardley, J. T.; Wei, Y. Chem Mater 1996, 8, 2701.
12. Yeh, J. M.; Liou, S. J.; Lin, C. Y.; Cheng, C. Y.; Chang, Y. W.; Lee, K. R. Chem Mater 2002, 14, 154.
13. Dybal, J.; Krimm, S. Macromolecules 1990, 23, 1301.
14. Wang, H.; Xu, P.; Zhong, W.; Shen, L.; Du, Q. Polym Degrad Stab 2005, 87, 319.
15. Gunji, T.; Makabe, Y.; Takamura, N.; Abe, Y. Appl Organomet Chem 2001, 15, 683.
16. Callister, W. D., Jr. Material Science and Engineering: An Introduction; Wiley: New York.
17. Li, D.; Huxtable, S. T.; Abramson, A. R.; Majumdar, A. J Heat Transfer 2005, 127, 108.
18. Ribbe, A.; Prucker, O. J Polym 1996, 37, 1087.
19. Yeh, J. M.; Liou, S. J.; Lai, C. Y.; Wu, P. C.; Tsai, T. Y. Chem Mater 2001, 13, 1131.
20. Yeh, J. M.; Liou, S. J.; Lai, M. C.; Chang, Y. W.; Huang, C. Y.; Chen, C. P.; Jaw, J. H.; Tsai, T. Y.; Yu, Y. H. J Appl Polym Sci 2004, 94, 1936.
21. Wei, Y.; Jin, D.; Brennan, D. J.; Rivera, D. N.; Zhuang, Q.; DiNardo, N. J.; Qiu, K. Chem Mater 1998, 10, 769.